T_c up to 23.6 K and robust superconductivity in the transition metal δ-Ti phase at megabar pressure

Xuqiang Liu,[1,2,*] Peng Jiang,[3,*] Yiming Wang,[2] Mingtao Li,[2] Nana Li,[2] Qian Zhang,[2,4] Yandong Wang,[1] Yan-Ling Li,[3,†] and Wenge Yang[2,‡]

[1]*Key Laboratory for Anisotropy and Texture of Materials, Northeastern University, Shenyang 110819, China*
[2]*Center for High Pressure Science and Technology Advanced Research, Shanghai 201203, China*
[3]*School of Physics and Electronic Engineering, Jiangsu Normal University, Xuzhou 221116, China*
[4]*School of Materials and Chemical Engineering, Zhongyuan University of Technology, Zhengzhou 451191, China*

(Received 1 December 2021; revised 17 May 2022; accepted 27 May 2022; published 21 June 2022)

We report a high superconducting transition temperature T_c up to 23.6 K, renewing the highest value in transition metals, under high pressure in the elemental metal Ti, one of the top ten most abundant elements in the earth's crust. The T_c increases monotonically from 2.3 K at 40.3 GPa to 23.6 K at 144.9 GPa. With further compression, a robust T_c of ∼23 K is observed between 144.9 and 183 GPa in the δ-Ti phase. The pressure-dependent T_c can be well described by the conventional electron-phonon coupling (EPC) mechanism. Density functional theory calculations show the Fermi nesting and the phonon softening of optical branches at the γ-Ti to δ-Ti phase transition pressure-enhanced EPC, which results in the high T_c. We attribute the robust superconductivity in δ-Ti to the apparent robustness of its strong EPC against lattice compression. These results provide insight into exploring high-T_c elemental metals and Ti-based superconducting alloys.

DOI: 10.1103/PhysRevB.105.224511

I. INTRODUCTION

Discovering materials with a high T_c is an active interest in condensed matter physics [1–6]. Simple superconducting elements are the original and most suitable platform on which to prove the Bardeen-Cooper-Schrieffer (BCS) theory [7,8]. To date, over 50 elements at ambient and high pressure have been discovered to host superconductivity [9] and more attention has particularly been paid to the transition metals (TMs). At ambient conditions, most TMs with partially filled d orbitals are superconductors [10]. By applying pressure, a remarkable increase of T_c has been found in some TMs such as scandium [11–14], yttrium [15–18], and vanadium [19–21]. Beyond TMs, calcium is believed so far to have the highest T_c near 21 K (accompanied by a superconductivity fluctuation at 29 K) among all elemental metals at ∼216 GPa, where Ca-VI (*Pnma*) transforms to Ca-VII (host-guest structure) [10,22–24]. The underlying mechanism of pressure-enhanced T_c in Ca [25,26], Sc [27,28], Y [17,29], and V [30] has been explained by electron-phonon coupling (EPC) or spin fluctuation, which is closely associated with the common s-d electron transfer [31–34]. Their maximum T_c ($T_c^{\max}$) probably correlates with the completion degree of the $s \to d$ transfer. For Ca, $T_c^{\max}$ appears in a complex host-guest structure [23], similar to the Ba-VI structure with the near completion of the $s \to d$ transfer [35]. A study of the T_c-dependent number of d electrons in the conduction band (N_d) for Sc and Y developed a phenomenological model where T_c approaches a saturated value once the $s \to d$ transfer is completed as the $N_d \to 3$ rule [11]. Also, a theoretical study reported that $T_c^{\max}$ appears at $N_d \sim 4$ in V under pressure of 139.3 GPa and T_c then decreases as N_d approaches 5 with the half-filled nature of its d orbital [30]. Hence, one intuitively expects that the pressure-induced $s \to d$ transfer in group IVB TMs with the electronic configuration $nd^2(n+1)s^2$ may reach a considerably high T_c.

As one of the group IVB TMs adjacent to the high-T_c Ca, Sc, V, and Y, pressurized titanium undergoes a structural transition sequence α ($P6_3/mmc$) $\to$ ω ($P6/mmm$) $\to$ γ ($Cmcm$) $\to$ δ ($Cmcm$) $\to$ β ($Im3m$) [36–42], where the γ and δ phases do not occur in pressurized zirconium [43–45] and hafnium [46,47]. Unlike the α and ω phases, the β phase in Zr and Hf has a negative slope of dT_c/dP [45,48]. The $T_c^{\max}$ of β-Zr appears at 33 GPa with $N_d = 3.5$ [45]. This leads us to infer that the occurrence of the β phase in group IVB TMs signals the completion of the $s \to d$ transfer, simultaneously triggering a $T_c^{\max}$. For Ti, interestingly, the γ and δ phases sequentially appear in a large pressure interval (over 100 GPa) before transforming into the β phase [36,37]. Thus, we expect that the broad interval is a promising fertile ground for obtaining high-T_c superconductivity in Ti. Indeed the T_c of ω-Ti was reported to slightly increase from 2.3 K at 40.9 GPa to 3.4 K at 56.0 GPa [49]. However, such a small positive dT_c/dP has not triggered further transport measurements at higher pressures. Up to now, the T_c in the γ-Ti and δ-Ti phases has remained absent from both experimental observations and theoretical predications. This motivated us to extend the transport measurements of Ti beyond megabar pressure.

In this work we present a comprehensive study of the superconducting behavior up to the δ-Ti phase near 2 Mbar. Interestingly, our results show that the $T_c^{\max}$ reaches 23.6 K at a pressure of about 145 GPa, renewing the highest value in TMs. After that, the T_c becomes nearly saturated in the pressure range of 145–183 GPa, manifesting robust superconductivity. Furthermore, theoretical calculations identify that

*These authors contributed equally to this work.
†ylli@jsnu.edu.cn
‡yangwg@hpstar.ac.cn

the conventional EPC mechanism can capture the evolution of the T_c in pressurized Ti well.

II. RESULTS AND DISCUSSION

Our experimental methods are described in detail in the Supplemental Material [50]. The diamond Raman method was used to determine the pressure in high-pressure electrical transport measurements [51]. The temperature-dependent resistance $R(T)$ measurements up to 183 GPa are plotted in Fig. 1(a). All $R(T)$ data show metallic behavior in the normal state. The bottom right inset displays a representative definition of the T_c at 183 GPa, in which the intersection signals the superconducting transition at $T_c = 23$ K. The close-up view of the $R(T)$ in the low-temperature region [Fig. 1(b)] shows a sharp drop occurring at 2.3 K and 40.3 GPa. This result is in line with the previous report [49]. The T_c shifts to a higher temperature with increasing pressure. Two noticeable drops in $R(T)$ are observed at 109.4 GPa, similar to the cases of Bi at 2.8 GPa and Ca at 193 GPa [22,52], indicating the coexistence of two superconducting phases. This might be mainly caused by the pressure gradient that is frequently present in ultrahigh pressure studies [53–55]. The magnetic field suppression of the superconducting transition in Fig. 1(c) shows two distinct slopes dH_{c2}/dT_c, which further supports the individual phases. At 130.3 GPa, the drop at a relatively lower temperature was gradually suppressed with increasing pressure. Based on previous studies [36–38,40,41,56,57], the phase transition regions in Ti of $\omega \rightarrow \gamma$ and $\gamma \rightarrow \delta$ were determined experimentally and theoretically to be 90–128 GPa and 106–140 GPa, respectively. Therefore, most of the sample had already transformed to δ-Ti, and the robust superconductivity beyond 140 GPa is within the δ-Ti phase. It should be noted that the bump around 6–7 K does not disappear completely until the pressure reaches 164.8 GPa, which could be mainly attributed to the presence of a strong pressure gradient in the sample.

To further confirm its superconducting nature, the suppression of superconducting transition was examined under a magnetic field. Figures 2(a)–2(c) show the magnetic field dependence of the superconducting transition at 59.3, 90, and 183 GPa, respectively. The transition is gradually suppressed by the magnetic field, supporting the superconductivity behavior rather than other transition origins. In Fig. 2(d), the external magnetic field–dependent T_c at 183 GPa follows the Ginzburg-Landau (GL) formula $\mu_0 H_{c2}(T) = \mu_0 H_{c2}(0)\{[1 - (T/T_c)^2]/[1 + (T/T_c)^2]\}$ [58], yielding the upper critical field $\mu_0 H_{c2}$ about 12.6 T at 0 K. The Werthamer-Helfand-Hohenberg equation [59] was also used to estimate the $\mu_0 H_{c2}(0)$, and the pressure dependence of $\mu_0 H_{c2}(0)$ is shown in Fig. S2 in [50].

The summarized T_c vs pressure is shown in Fig. 3(a). Initially, the T_c exhibits a slow increase from 2.3 K at ~40 GPa to 7.1 K at ~130 GPa. This demonstrates the previous assumption that the T_c for Ti can increase linearly to about 8.7 K when it transforms to the γ phase at ~128 GPa [49]. Until ~145 GPa, the T_c rises rapidly to 23.6 K with $dT_c/dP = 0.39$ K/GPa. The T_c of 23.6 K is the highest among TMs [see the $T_c^{\max}$ of Sc, Y, V, and Ti in Fig. 3(a)]. Note that at 216 GPa Ca shows a superconductivity fluctuation at 29 K, but the

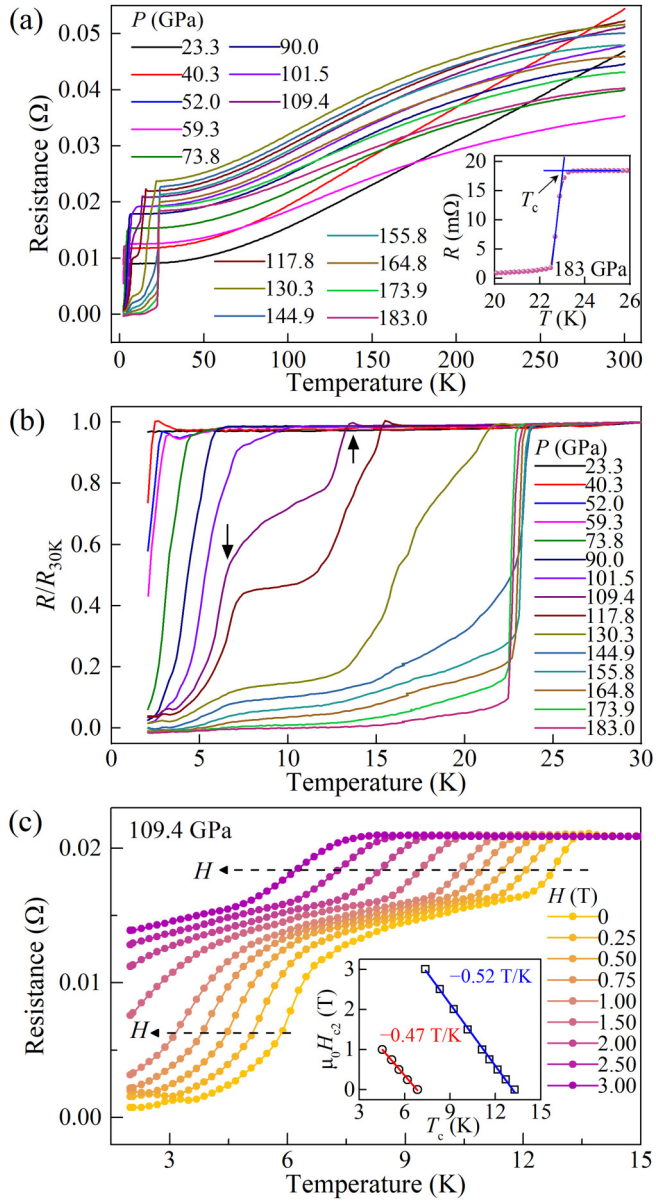

FIG. 1. (a) Temperature-dependent resistance $R(T)$ of Ti from 2 to 300 K at pressure up to 183 GPa. The inset shows the determination of the T_c at 183 GPa. (b) Close-up of the normalized resistance in the low-temperatures region in (a). The arrows indicate two possible superconducting transitions at 109.4 GPa. (c) Magnetic field dependence of the superconducting transition in Ti at 109.4 GPa. The inset displays the temperature dependence of the upper critical magnetic field.

rapid drop in resistance occurs at 21 K [22,62]. Therefore, the $T_c^{\max} = 23.6$ K in Ti is a high value for elemental superconductors. With further increasing pressure up to 183 GPa, the T_c remains almost constant at 23 K. Such a robust T_c surviving over megabar pressure is also observed in some Ti-bearing alloys, such as NbTi wire [54] and high-entropy alloy $(TaNb)_{0.67}(HfZrTi)_{0.33}$ [63].

As shown in Fig. 3(a), the $T_c(P)$ for Y, V, and Ca show monotonically increasing behavior without interruption through the phase boundary. For Sc, the appearance of the Sc-III phase causes the T_c to decrease significantly, but it still

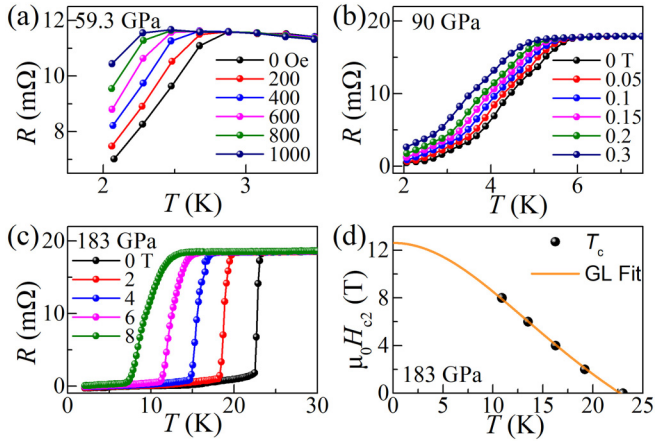

FIG. 2. Temperature-dependent resistance of Ti under different magnetic fields at (a) 59.3, (b) 90, and (c) 183 GPa. (d) Temperature-dependent $\mu_0 H_{c2}$ at 183 GPa. The yellow curve is plotted by fitting the GL formula.

maintains a positive dT_c/dP with further compression [11]. In contrast, the T_c of Ti is more sensitive to the changes in the crystal structure. The pressure-dependent T_c matches well with the structural transition sequence, which characterizes a different dT_c/dP and $\mu_0 H_{c2}(0)$ (see Fig. S2 in [50]).

We further performed density functional theory (DFT) calculations to elucidate the experimental observations in Ti. The theoretical details of the structure prediction method and DFT calculations are described in [50], which includes some important literature [64–71]. The relative enthalpies vs pressure of the overall phases are shown in Fig. S3 in [50]. The results indeed confirm the previously reported fact that Ti undergoes the $\alpha \rightarrow \omega \rightarrow \gamma \rightarrow \delta \rightarrow \beta$ phase transition at 80–250 GPa [36–42]. It is worth noting that the δ phase can gradually relax to the β phase at pressures $P > 170$ GPa, resulting in identical enthalpies for the δ phase and β phase. According to the McMillan-Allen-Dynes formula [7,8], the T_c can be estimated using three parameters: the effectively screened Coulomb repulsion constant μ^*, logarithmic average frequency $\omega_{\log}$, and EPC parameter λ. Here μ^* is fixed at 0.19, which is obtained by fitting the theoretically calculated λ and $\omega_{\log}$ at 50 GPa, and the experimental measured T_c at 56 GPa [49]. Then the obtained μ^* value is used to theoretically predict the T_c values of the different phases (ω, γ, δ, and β) of Ti at high pressure. Figure 3(b) plots the trend of the calculated T_c, which matches with the experimental results surprisingly well. In particular, the δ phase is predicted to host the most stable structure with a T_c of 23 K between 130 and 170 GPa. However, after entering the bcc β phase, the T_c begins to decrease when $P > 180$ GPa. Similar behavior is also observed in superconducting Zr under pressure [48]. To reveal the effect of μ^* on the theoretical T_c prediction, we plot the $T_c(P)$ at three μ^* values as shown in Fig. 3(b), which shows that T_c has a similar tendency with increasing pressure for different μ^*. Note that the T_c value of δ-Ti at 140 GPa is predicted to be around 21–26 K, with μ^* in the range of 0.16–0.22.

The calculated $\omega_{\log}$ and λ data are shown in Fig. 3(c). When γ-Ti appears at 100 GPa, $\omega_{\log}$ suddenly decreases. This abnormal frequency softening usually induces a sizable enhancement of λ [72], leading to the increase of T_c in γ-

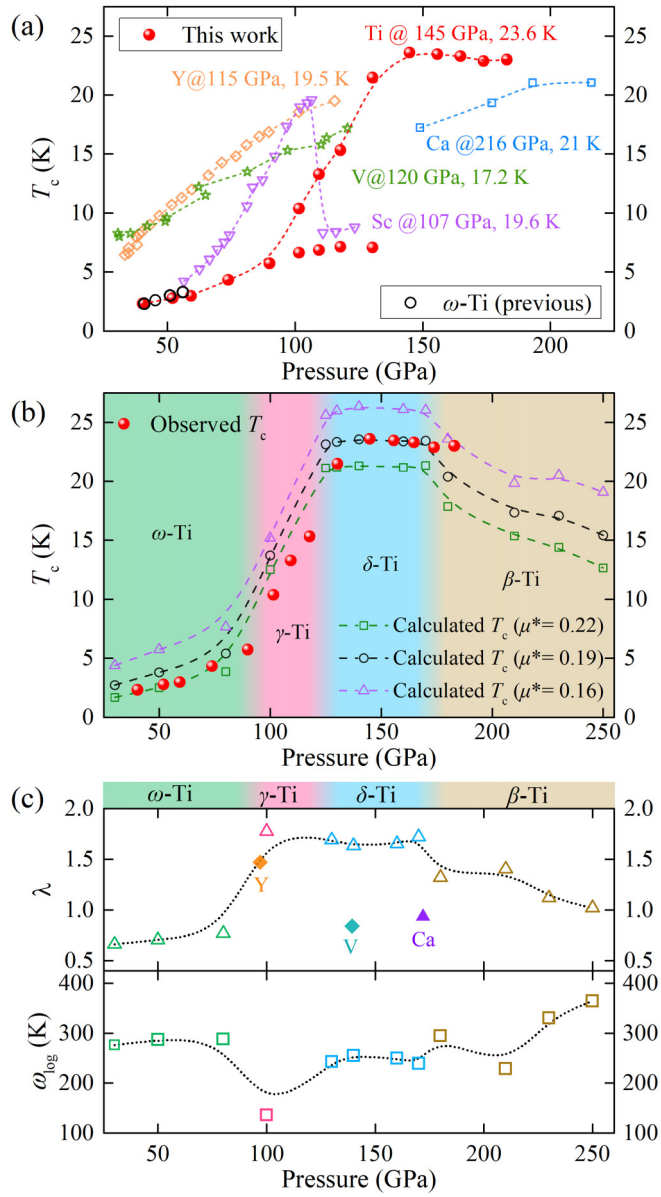

FIG. 3. (a) Observed T_c as a function of pressure for Ti up to 180 GPa. The closed and open circles represent results from the present work and previous data [49], respectively. The experimental $T_c^{\max}$ values for Sc, Y, V, and Ca are from Refs. [11,15,19,22]. (b) DFT calculation of T_c vs pressure using different μ^* for Ti up to 250 GPa. (c) Pressure dependence of the EPC parameter λ and logarithmic average frequency $\omega_{\log}$ calculated using the BCS and Migdal-Eliashberg theories [60,61]. The λ values of Y, V, and Ca are taken from previous works [17,26,30].

Ti. The calculated $\lambda \sim 1.65$ for δ-Ti at 130–170 GPa is the largest among the surrounding elements (Ca, Y, and V) near the pressure maximizing T_c. Experimentally, the T_c reaches a value of about 23.6 K at 144.9 GPa, verifying that the high T_c of Ti is mainly contributed by strong EPC. Above 180 GPa, the $\omega_{\log}$ of the β phase rises sharply upon compression. This drastic phonon hardening causes weakening of the electron-phonon interactions, usually accompanying a decline in λ [as shown in Fig. 3(b)]. Recent work has claimed to observe the β-Ti phase at 243 GPa [42]. Given that the

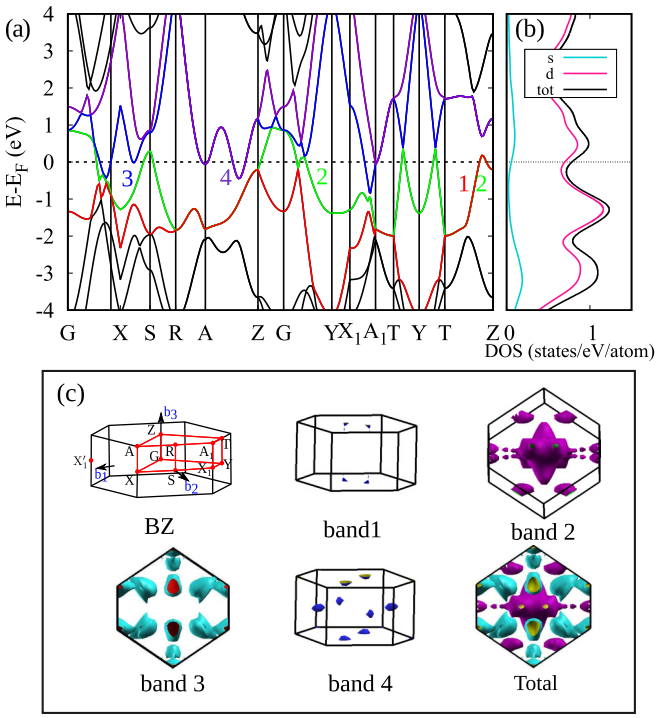

FIG. 4. (a) Band structure and (b) projected DOS of δ-Ti at 140 GPa. (c) First Brillouin zone (BZ) and band-projected Fermi surface of δ-Ti at 140 GPa.

present pressure range extends to 183 GPa, it remains uncertain whether the robust superconductivity against volume shrinkage (RSAVS) will persist at higher pressures. However, our theoretical prediction suggests a negative expectation. The RSAVS over megabar pressure is proposed to be extremely unusual and virtually unique among known superconductors [54,63,73]. Nevertheless, Jasiewicz *et al.* showed that the EPC mechanism can explain the RSAVS state observed in $(TaNb)_{0.67}(HfZrTi)_{0.33}$ [74]. Another theoretical calculation revealed that the RSAVS state is associated with the stability of partial density of states (DOS) contributed by the d-orbital electrons from all constituent atoms [75], which remain almost unchanged in the $(TaNb)_{0.67}(HfZrTi)_{0.33}$ and NbTi alloys.

It is well known that both the EPC strength and the DOS around the Fermi level E_F play important roles in the T_c enhancement in phonon-mediated superconductors. We calculated the pressure-dependent DOS at the Fermi level $N(E_F)$, as shown in Fig. S4 in [50]. The overall $N(E_F)$ decreases as pressure increases, but it reaches a local maximum at the γ-δ phase boundary. Combined with the increase in the EPC strength at the $\omega \rightarrow \gamma$ phase transition and a high plateau in the δ phase [see Fig. 3(c)], the T_c gives the highest value 23.6 K at the $\gamma \rightarrow \delta$ phase transition pressure and maintains it around 23 K for the rest of δ phase. This powerfully demonstrates that the high and robust T_c mainly arises from the enhanced EPC under pressure.

We took δ-Ti at 140 GPa as a representative case and calculated its band structure and orbital projected DOS to reveal the pressure-induced T_c enhancement mechanism. As shown in Figs. 4(a) and 4(b), four bands (1–4) cross the E_F along the high-symmetry k path in the Brillouin zone, indicating metallic nature in the δ-Ti phase. Note that bands 1 and 2 degenerate along the Z-T path. From the DOS and the orbital projected band structure shown in Fig. S5 in [50], the Ti d states mainly contribute to the bands around the E_F. Thus, the main physics of δ-Ti is essentially associated with the Ti d orbitals, and $N(E_F)$ is about 0.85 states/eV per atom.

To establish the origin of the high T_c of δ-Ti, we calculated its Fermi surface (FS) at 140 GPa, as shown in Fig. 4(c). The FS is made of four sections: four cone-shaped holelike pockets along the T-Z direction in band 1; a big four-point-star-shaped hole-like pockets around the G point, four horn-shaped holelike pockets around the S point, and four gear-shaped sheets around the T-Y path in band 2; electron-hole Fermi pockets formed by a dozen electronlike pockets around the A and A_1 points, four holelike pockets along the two X_1-X_1' paths perpendicular to the G-X path, and four horn-shaped electron sheets along the A-Z path in band 3; and four electronlike pockets along the A-Z path and four shuttle-shaped sheets along the two X_1-X_1' paths perpendicular to the G-X path in band 4. One key finding is that the FS nesting appears in some Fermi pockets, which substantially enhances the EPC and results in high-T_c superconductivity in δ-Ti [76,77].

Electron transferring from the s band to d band under pressure is well known as a common feature of transition metals in many theoretical calculations [11,30,31]. Following a similar approach, our extended Löwdin charge analysis also reveals a pressure-driven $s \rightarrow d$ transfer in Ti [see Fig. 5(a)]. The increase in N_d with pressure is caused by a relative increase in the energy of the s electrons compared to the d electrons with pressure increase or volume reduction [37]. Note that the rate of N_d increase slows down upon entering the γ phase, and the change in dN_d/dP is evident, almost halving. The equations of state have a response to this dip: The total volume reduction from ω to δ phase is 3.0% at 147 GPa [36]. In addition, the high T_c was experimentally observed at 144.9 GPa. Hence, this dip in dN_d/dP may approach the completion of the $s \rightarrow d$ transfer and the high T_c is reached as we expect. Overall, by combining experiments with theoretical calculations, we demonstrate the connection between the $s \rightarrow d$ transfer and superconductivity in Ti, calling for electronic structure calculations to check whether the same scenario works in other high-T_c TMs.

The phonon spectrum, Eliashberg spectral function $\alpha^2F(\omega)$, and cumulative $\lambda(\omega)$ of δ-Ti were calculated to investigate the lattice dynamics and electron-phonon interactions of the δ phase, as shown in Figs. 5(b) and 5(c). The absence of imaginary phonon modes demonstrates its thermodynamical stability at 140 GPa, which agrees with previous studies [41]. The phonon linewidth [denoted by the dots in Fig. 5(b)] is plotted on the phonon dispersion curve to gain further insight into the nature of the EPC. The main considerable contribution to the EPC strength is the optical branches based on the calculated phonon linewidths. Note that the optical branches are dominated by three Raman modes designated by B_{1g}, A_g, and B_{3g}. The results show that the low-frequency (below 120 cm^{-1}) vibration only contributes 20.2% of the total EPC constant λ, which is largely caused by the softening of the lowest acoustic branch along the S-R-A, Z-G, and X_1-Y paths. This means that the dominant contributions

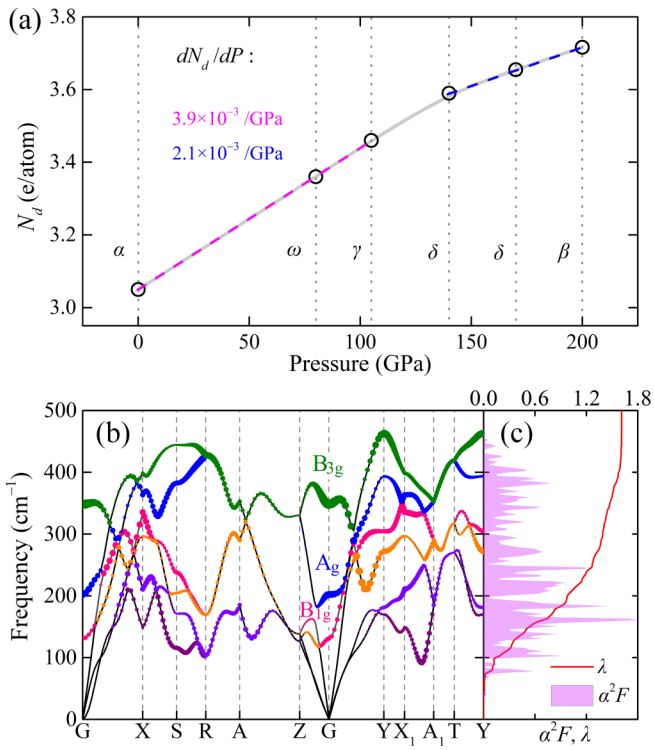

FIG. 5. (a) Charge number of d orbitals for Ti as a function of pressure. The results at 0, 80, 105, 140, and 200 GPa were obtained in the α, ω, γ, δ, and β phases, respectively. (b) Phonon dispersion of δ-Ti at 140 GPa. The different colors denote the different phonon branches. The dots are proportional to the strengths of the phonon linewidth. (c) Eliashberg spectral function $\alpha^2F(\omega)$ and cumulative frequency-dependent EPC function $\lambda(\omega)$.

to λ stem from the medium- and high-frequency vibrations. It is consistent with the fact that the frequency of the highest optical mode B_{3g} provides the largest linewidth, followed by the A_g and B_{1g} modes around the G point. All Raman modes exhibit phonon softening along other high-symmetry k paths, indicating a strong EPC in δ-Ti. Unlike the simple alkaline-earth metals, in which $N(E_F)$ is dominated by s states, the T_c of TMs usually exhibits a highly nonlinear dependent T_c on pressure [11]. Such complexity is associated with the nature of their partially filled d electrons and phase transition under pressure [11,78], which is consistent with our results.

III. CONCLUSION

In summary, we have reported the observation of a high T_c of 23.6 K and robust superconductivity in the δ-Ti phase between 144.9 and 183 GPa. The unusual superconductivity in pressurized Ti can be explained by the scenario of the strong electron-phonon coupling effect from Fermi nesting formed by holelike and electronlike Fermi pockets and the substantial phonon softening of its optical modes. Our results provide in-depth insight into the understanding of the pressure-tuning superconductivity of transition metals, which is fundamentally important for the design and synthesis of high-T_c titanium alloy superconductors for applications at extreme conditions.

Note added. Recently, a similar study of superconductivity measurements in titanium was reported, which reproduced the T_c-P phase diagram [79], further validating this discovery of high-T_c superconductivity in this system.

ACKNOWLEDGMENTS

The authors thank Dr. Zhipeng Yan, Dr. Cheng Ji, Dr. Junyue Wang, and Dr. Dayong Liu for their technical support and theory guidance. We acknowledge support from the National Natural Science Foundation of China through Grants No. U1930401, No. 11804011, No. 12074153, No. 51527801, and No. 11674131. P.J. acknowledge the project funded by Jiangsu Normal University under Grant No. 21XSRS006.

[1] M. K. Wu, J. R. Ashburn, C. J. Torng, P. H. Hor, R. L. Meng, L. Gao, Z. J. Huang, Y. Q. Wang, and C. W. Chu, Phys. Rev. Lett. **58**, 908 (1987).
[2] A. P. Drozdov, M. I. Eremets, I. A. Troyan, V. Ksenofontov, and S. I. Shylin, Nature (London) **525**, 73 (2015).
[3] M. Somayazulu, M. Ahart, A. K. Mishra, Z. M. Geballe, M. Baldini, Y. Meng, V. V. Struzhkin, and R. J. Hemley, Phys. Rev. Lett. **122**, 027001 (2019).
[4] E. Snider, N. Dasenbrock-Gammon, R. McBride, M. Debessai, H. Vindana, K. Vencatasamy, K. V. Lawler, A. Salamat, and R. P. Dias, Nature (London) **586**, 373 (2020).
[5] L. Zhang, Y. Wang, J. Lv, and Y. Ma, Nat. Rev. Mater. **2**, 17005 (2017).
[6] H.-K. Mao, B. Chen, H. Gou, K. Li, J. Liu, L. Wang, H. Xiao, and W. Yang, Matter Radiat. Extrem. **6**, 013001 (2021).
[7] W. L. McMillan, Phys. Rev. **167**, 331 (1968).
[8] P. B. Allen and R. C. Dynes, Phys. Rev. B **12**, 905 (1975).
[9] K. Shimizu, Physica C **552**, 30 (2018).
[10] J. Hamlin, Physica C **514**, 59 (2015).
[11] M. Debessai, J. J. Hamlin, and J. S. Schilling, Phys. Rev. B **78**, 064519 (2008).
[12] Y. Akahama, H. Fujihisa, and H. Kawamura, Phys. Rev. Lett. **94**, 195503 (2005).
[13] H. Fujihisa, Y. Akahama, H. Kawamura, Y. Gotoh, H. Yamawaki, M. Sakashita, S. Takeya, and K. Honda, Phys. Rev. B **72**, 132103 (2005).
[14] M. I. McMahon, L. F. Lundegaard, C. Hejny, S. Falconi, and R. J. Nelmes, Phys. Rev. B **73**, 134102 (2006).
[15] J. Hamlin, V. Tissen, and J. Schilling, Physica C **451**, 82 (2007).
[16] E. J. Pace, S. E. Finnegan, C. V. Storm, M. Stevenson, M. I. McMahon, S. G. MacLeod, E. Plekhanov, N. Bonini, and C. Weber, Phys. Rev. B **102**, 094104 (2020).
[17] Y. Chen, Q.-M. Hu, and R. Yang, Phys. Rev. Lett. **109**, 157004 (2012).
[18] Y. Deng and J. S. Schilling, Phys. Rev. B **99**, 085137 (2019).
[19] M. Ishizuka, M. Iketani, and S. Endo, Phys. Rev. B **61**, R3823 (2000).
[20] Y. Ding, R. Ahuja, J. Shu, P. Chow, W. Luo, and H.-K. Mao, Phys. Rev. Lett. **98**, 085502 (2007).
[21] N. Suzuki and M. Otani, J. Phys.: Condens. Matter **14**, 10869 (2002).

[22] M. Sakata, Y. Nakamoto, K. Shimizu, T. Matsuoka, and Y. Ohishi, Phys. Rev. B **83**, 220512(R) (2011).
[23] H. Fujihisa, Y. Nakamoto, M. Sakata, K. Shimizu, T. Matsuoka, Y. Ohishi, H. Yamawaki, S. Takeya, and Y. Gotoh, Phys. Rev. Lett. **110**, 235501 (2013).
[24] T. Yabuuchi, T. Matsuoka, Y. Nakamoto, and K. Shimizu, J. Phys. Soc. Jpn. **75**, 083703 (2006).
[25] G. Gao, Y. Xie, T. Cui, Y. Ma, L. Zhang, and G. Zou, Solid State Commun. **146**, 181 (2008).
[26] M. Aftabuzzaman and A. K. M. A. Islam, J. Phys.: Condens. Matter **23**, 105701 (2011).
[27] L. W. Nixon, D. A. Papaconstantopoulos, and M. J. Mehl, Phys. Rev. B **76**, 134512 (2007).
[28] S. K. Bose, J. Phys.: Condens. Matter **20**, 045209 (2008).
[29] S. Lei, D. A. Papaconstantopoulos, and M. J. Mehl, Phys. Rev. B **75**, 024512 (2007).
[30] C. N. Louis and K. Iyakutti, Phys. Rev. B **67**, 094509 (2003).
[31] H. L. Skriver, Phys. Rev. B **31**, 1909 (1985).
[32] A. McMahan, Physica B+C **139–140**, 31 (1986).
[33] D. G. Pettifor, J. Phys. F **7**, 613 (1977).
[34] G. B. Grad, P. Blaha, J. Luitz, K. Schwarz, A. Fernández Guillermet, and S. J. Sferco, Phys. Rev. B **62**, 12743 (2000).
[35] I. Loa, R. Nelmes, L. Lundegaard, and M. McMahon, Nat. Mater. **11**, 627 (2012).
[36] Y. Akahama, H. Kawamura, and T. Le Bihan, Phys. Rev. Lett. **87**, 275503 (2001).
[37] Y. K. Vohra and P. T. Spencer, Phys. Rev. Lett. **86**, 3068 (2001).
[38] A. L. Kutepov and S. G. Kutepova, Phys. Rev. B **67**, 132102 (2003).
[39] R. Ahuja, L. Dubrovinsky, N. Dubrovinskaia, J. M. O. Guillen, M. Mattesini, B. Johansson, and T. Le Bihan, Phys. Rev. B **69**, 184102 (2004).
[40] Y. Hao, J. Zhu, L. Zhang, J. Qu, and H. Ren, Solid State Sci. **12**, 1473 (2010).
[41] A. Dewaele, V. Stutzmann, J. Bouchet, F. Bottin, F. Occelli, and M. Mezouar, Phys. Rev. B **91**, 134108 (2015).
[42] Y. Akahama, S. Kawaguchi, N. Hirao, and Y. Ohishi, J. Appl. Phys. **128**, 035901 (2020).
[43] H. Xia, S. J. Duclos, A. L. Ruoff, and Y. K. Vohra, Phys. Rev. Lett. **64**, 204 (1990).
[44] J. C. Jamieson, Science **140**, 72 (1963).
[45] Y. Akahama, M. Kobayashi, and H. Kawamura, J. Phys. Soc. Jpn. **60**, 3211 (1991).
[46] H. Xia, G. Parthasarathy, H. Luo, Y. K. Vohra, and A. L. Ruoff, Phys. Rev. B **42**, 6736 (1990).
[47] J. S. Gyanchandani, S. C. Gupta, S. K. Sikka, and R. Chidambaram, J. Phys.: Condens. Matter **2**, 6457 (1990).
[48] Y. Akahama, M. Kobayashi, and H. Kawamura, J. Phys. Soc. Jpn. **59**, 3843 (1990).
[49] I. Bashkin, V. Tissen, M. Nefedova, and E. Ponyatovsky, Physica C **453**, 12 (2007).
[50] See Supplemental Material at http://link.aps.org/supplemental/10.1103/PhysRevB.105.224511 for experimental and computational details; pressure dependence of upper critical field; the enthalpies difference of the four phases in Ti as a function of pressure; pressure-dependent DOS at Fermi level; orbital projected band structure of δ-Ti phase at 140 GPa.
[51] Y. Akahama and H. Kawamura, J. Appl. Phys. **100**, 043516 (2006).
[52] Y. Li, E. Wang, X. Zhu, and H.-H. Wen, Phys. Rev. B **95**, 024510 (2017).
[53] D. Errandonea, Y. Meng, M. Somayazulu, and D. Häermann, Physica B **355**, 116 (2005).
[54] J. Guo, G. Lin, S. Cai, C. Xi, C. Zhang, W. Sun, Q. Wang, K. Yang, A. Li, Q. Wu, Y. Zhang, T. Xiang, R. J. Cava, and L. Sun, Adv. Mater. **31**, 1807240 (2019).
[55] S. G. MacLeod, B. E. Tegner, H. Cynn, W. J. Evans, J. E. Proctor, M. I. McMahon, and G. J. Ackland, Phys. Rev. B **85**, 224202 (2012).
[56] A. K. Verma, P. Modak, R. S. Rao, B. K. Godwal, and R. Jeanloz, Phys. Rev. B **75**, 014109 (2007).
[57] Y.-J. Hao, L. Zhang, X.-R. Chen, Y.-H. Li, and H.-L. He, Solid State Commun. **146**, 105 (2008).
[58] M. Tinkham, Phys. Rev. **129**, 2413 (1963).
[59] N. R. Werthamer, E. Helfand, and P. C. Hohenberg, Phys. Rev. **147**, 295 (1966).
[60] J. Bardeen, L. N. Cooper, and J. R. Schrieffer, Phys. Rev. **108**, 1175 (1957).
[61] F. Giustino, Rev. Mod. Phys. **89**, 015003 (2017).
[62] M. Andersson, Phys. Rev. B **84**, 216501 (2011).
[63] J. Guo, H. Wang, F. von Rohr, Z. Wang, S. Cai, Y. Zhou, K. Yang, A. Li, S. Jiang, Q. Wu, R. J. Cava, and L. Sun, Proc. Natl. Acad. Sci. USA **114**, 13144 (2017).
[64] A. R. Oganov, A. O. Lyakhov, and M. Valle, Acc. Chem. Res. **44**, 227 (2011).
[65] A. O. Lyakhov, A. R. Oganov, H. T. Stokes, and Q. Zhu, Comput. Phys. Commun. **184**, 1172 (2013).
[66] P. Giannozzi, S. Baroni, N. Bonini, M. Calandra, R. Car, C. Cavazzoni, D. Ceresoli, G. L. Chiarotti, M. Cococcioni, I. Dabo, A. D. Corso, S. de Gironcoli, S. Fabris, G. Fratesi, R. Gebauer, U. Gerstmann, C. Gougoussis, A. Kokalj, M. Lazzeri, L. Martin-Samos *et al.*, J. Phys.: Condens. Matter **21**, 395502 (2009).
[67] P. E. Blöchl, Phys. Rev. B **50**, 17953 (1994).
[68] G. Kresse and J. Furthmüller, Phys. Rev. B **54**, 11169 (1996).
[69] G. Kresse and D. Joubert, Phys. Rev. B **59**, 1758 (1999).
[70] D. R. Hamann, Phys. Rev. B **88**, 085117 (2013).
[71] S. Baroni, S. de Gironcoli, A. Dal Corso, and P. Giannozzi, Rev. Mod. Phys. **73**, 515 (2001).
[72] X.-J. Chen, Matter Radiat. Extrem. **5**, 068102 (2020).
[73] L. Sun and R. J. Cava, Phys. Rev. Materials **3**, 090301 (2019).
[74] K. Jasiewicz, B. Wiendlocha, K. Górnicka, K. Gofryk, M. Gazda, T. Klimczuk, and J. Tobola, Phys. Rev. B **100**, 184503 (2019).
[75] C. Huang, J. Guo, J. Zhang, K. Stolze, S. Cai, K. Liu, H. Weng, Z. Lu, Q. Wu, T. Xiang, R. J. Cava, and L. Sun, Phys. Rev. Materials **4**, 071801(R) (2020).
[76] D. Kasinathan, J. Kuneš, A. Lazicki, H. Rosner, C. S. Yoo, R. T. Scalettar, and W. E. Pickett, Phys. Rev. Lett. **96**, 047004 (2006).
[77] Y. L. Li, W. Luo, X. J. Chen, Z. Zeng, H. Q. Lin, and R. Ahuja, Sci. Rep. **3**, 3331 (2013).
[78] S.-C. Zhu, X.-Z. Yan, S. Fredericks, Y.-L. Li, and Q. Zhu, Phys. Rev. B **98**, 214116 (2018).
[79] C. L. Zhang, X. He, C. Liu, Z. W. Li, K. Lu, S. J. Zhang, S. M. Feng, X. C. Wang, Y. W. Long, L. H. Wang, M. Y. Ye, V. B. Prakapenka, S. Chariton, Q. Li, Y. M. Ma, H. Z. Liu, C. F. Chen, and C. Q. Jin, arXiv:2112.12396.